

Supporting Information

Carrier Recombination and Plasmonic Emission Channels in Metallic Photoluminescence

Jiyong Wang, Emre Gürdal, Anke Horneber, Simon Dickreuter, Sergei Kostcheev, Alfred J. Meixner, Monika Fleischer, Pierre-Michel Adam * Dai Zhang *

1. Sample fabrication

After being cleaned by acetone and isopropanol in an ultrasonic bath, the substrate (145µm thick glass slide with a 60nm ITO layer) was coated with a layer of electron-sensitive resist (Poly-Methyl-Metacrylate (PMMA) 950K diluted in Methyl-Iso-Butyl-Ketone (MIBK) at 30g/L in a spin-coater (spinning speed: 3000 rpm, acceleration speed: 4000 rpm/s, duration: 30 s). The thickness of the resist is expected to be 160 nm, according to the empirical curve of the spinning speed versus the film thickness. After soft baking (convection oven at 170 °C for 3 h), the resist was exposed with the pre-designed patterns by the electron beam. The written patterns were developed by a solution of MIBK (diluted with isopropanol with a ratio of 1:3). In the development process, the exposed areas of the resist were removed. Then a physical vapor deposition (PVD) process was used to coat the sample with a 2 nm thick Cr layer (for adhesion purposes) and a 50 nm thick Au layer. The sample was finally immersed in acetone for more than 3 h to lift-off the remaining resist. The conducting transparent ITO layer, which is however insulating at optical frequencies, is chosen to facilitate imaging of the nanostructures by scanning electron microscopy.

2. Nonlinear optical measurements

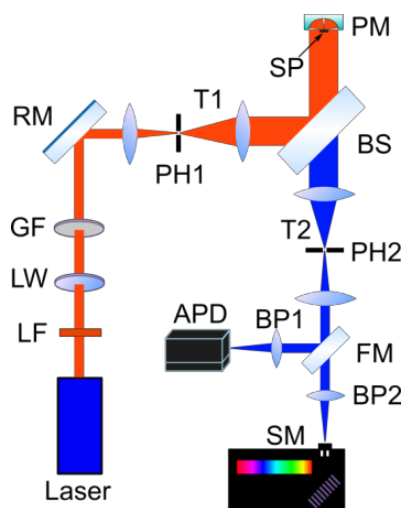


Figure S1. Sketch of the nonlinear optical setup based on a parabolic mirror. LF: Laser line filter; LW: lambda-half wave-plate; GF: gradient filter; RM: reflecting mirror; T1, 2: telescopes; PH1,2 : pinhole; BS: beam splitter; PM: parabolic mirror; SP: Sample; FM: flipping mirror; BP1,2: Band-pass filter; APD: avalanche photo-diode; SM: spectrometer. For the non-linear measurements, the incident light is supplied by a femtosecond pulse laser (~110 fs, 89 MHz) with a wavelength centered at 774 nm. The transmission rate can be tuned from 0 to 100% by a gradient neutral density filter.

Figure S1 shows the optical path of the confocal optical microscope. A femtosecond laser (TOPTICA PHOTONICS) generates ultra-short pulses (~ 110 fs, 89 MHz, 774 nm) in a TEM₀₀ Gaussian mode and was employed to excite the sample. The output power of the laser is 500 pJ/pulse. The incident beam passed through a gradient grey filter and a lambda-half wave plate, being able to tune the incident power and excitation polarization, respectively. Afterwards the beam was expanded by a telescope. By using a pinhole within the telescope, undesired and scattered light was filtered out to obtain a homogeneous Gaussian mode. The linearly polarized light was reflected by a non-polarizing dichroic beam splitter towards the parabolic mirror. The parabolic mirror serves both as the focusing element and the emission collector. In air its NA reaches 0.998.¹ Such a high-NA and low-chromatic-aberration mirror enables a high resolution down to the diffraction limit. The emitted optical signal of the nanoparticles was collected and sent through the beam splitter. The dichroic beam splitter excludes the light at the fundamental and higher wavelengths and only transmits the non-linear information. After reducing the beam size with a second telescope, scattered light is excluded by a pin-hole, and the detection wavelength range was selected by a band-pass filter (370 nm - 700 nm). With a flipping mirror, the beam was either directed towards the spectrometer (Princeton Instruments) to obtain spectral information or to an APD (Single Photon Counting Module - COUNT® BLUE) for point-by-point imaging.

The nonlinear background signals (see Figure S2) originating from glass and ITO are subtracted from our measurements shown in the manuscript. The background also exhibits some weak nonlinear signal (see the slight SHG peak at 387 nm), which is however negligible compared to the signal observed from the nanostructures.

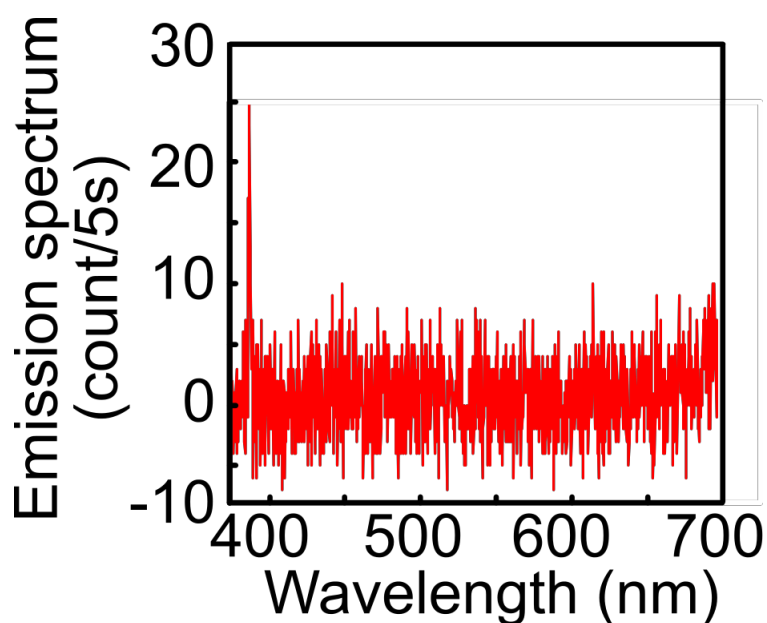


Figure S2. Nonlinear emission from the ITO/glass substrate

3. Dark-field scattering measurements

Dark-field scattering spectroscopy was employed to measure the linear optical properties of the Au NPs. The sample, placed on an inverted microscope (Nikon Ti-U), was illuminated from the substrate side by a halogen lamp through a dark-field condenser (NA 0.8-0.95). The scattered light coming from the nano-structures was collected from the airside by a 60x objective with a numerical aperture (NA) of 0.7 and sent to a spectrometer (Ocean Optics QE 65000) through a pin-hole, by which the signal from a circular section of the image plane with a diameter of 3.33 μm was collected. The measured intensity curves were background corrected (using intensity curves measured in an unstructured area of the sample) and normalized by dividing by the (dark-current corrected) lamp spectrum.

4. Scattering simulations

Scattering spectra were simulated by means of the (boundary element method-based) MNPBEM toolbox.² We simulated 50 nm thick gold single nanodiscs with diameters ranging from 80 nm to 190 nm in 10 nm steps on a substrate of refractive index $n=1.6$. The refractive index corresponds to an intermediate value between those of an ITO film and an ITO surface layer in the observed wavelength range according to literature.³ The authors are aware that the refractive index of ITO is both wavelength and preparation dependent. The value of 1.6 provides good agreement with the measured spectra and shows the general trend for increasing disk sizes. Deviations of n would lead to minor gradual shifts in the peak position. The permittivity of gold was taken from literature.⁴ The particles simulated in Figure 2(b) are excited with white light in a spectral range from 500 nm to 850 nm in 5 nm steps with an incident angle of 33° (Snell's law for incidence from the substrate side, corresponding to the average angle of the dark-field condenser of 60° (NA 0.8-0.95)). Since unpolarized light was used in the measurements, two sets of simulations were performed for TM and TE polarized light. In the Figure the results are superposed as $(I_{\text{TM}}+I_{\text{TE}})/2$. In the model system the far-field scattering spectra were calculated by integrating the Poynting vector on the air side from 0° to 45° , in analogy to the 60x objective with a NA of 0.7. The edges on the top of the particles were rounded with a 10 nm radius, and a maximum element size of the mesh of 7 nm was used.

5. Integrated MPL intensity from emission mode 1

The shifting emission mode of MPL is firstly fitted by a Gaussian function:

$$f(x) = ae^{-\frac{(x-b)^2}{2c^2}}$$

where a denotes the amplitude and b the peak position. $\text{FWHM} = 2\sqrt{2\ln 2}c$. The integral of a Gaussian function over the whole real line can be calculated as:

$$I = \int_{-\infty}^{+\infty} f(x) dx = ac \cdot \sqrt{2\pi}$$

6. Extraction of the e-h pair emission modes

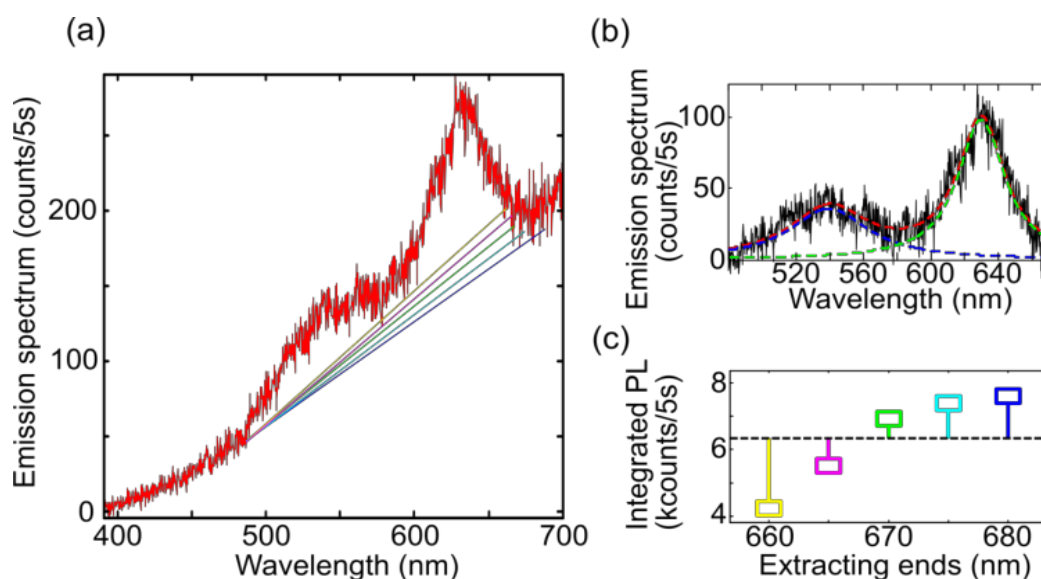
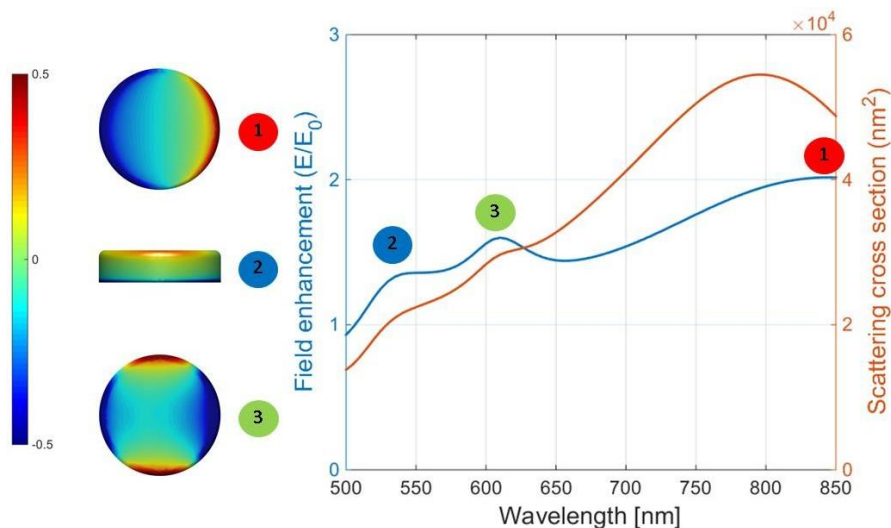


Figure S3. (a) Original emission spectrum of an Au disc with a diameter of 185 nm. The e-h pair radiation modes can be extracted by subtracting the tail of the PP emission mode, approximated by linearly subtracting the background. The extracting start is always set at 480 nm, as it is on the level of the linearly increasing background. Since the background level at the upper end of the spectrum is less clearly identifiable, the extracting ends are varied between 660 nm (yellow), 665 nm (magenta), 670 nm (green), 675 nm (cyan) and 680 nm (blue). (b) Example for fitting the extracted e-h pair mode MPL is shown. The extracted PL spectrum (black line) ranges from 480 to 670 nm, and it is fitted by two Lorentzian functions (red dashed line), as a superposition of two separated peaks situated at 540 nm (blue dashed line) and 630 nm (green dashed line). (c) Integrated PL of the fitted spectra from 5 extracting ranges, which correspond to the ones in (a). The averaged value (black dashed horizontal line) is regarded as the intensity of the e-h pair mode for this Au disc size. The biggest and smallest values are regarded as the upper and lower errors in the error bar.

7. Involvement of further plasmon modes



FigureS4. Simulated far-field scattering spectrum (orange line) and simulated near-field enhancement spectrum (blue line) of a 190 nm diameter disc, showing three discernible plasmonic modes and the respective charge distributions at the disc surface (side view for the vertical mode at ~540nm, bottom views for the quadrupolar mode at ~610 nm and the dipolar mode at ~795 nm in the far-field scattering spectrum and ~850 nm in the near-field enhancement spectrum).

Several peaks appear in the numerically simulated far-field scattering and near-field enhancement spectrum of a 190 nm gold disc. The particle was excited from the air side with white light (TM polarized) at an incident angle of 60° , and (in contrast to Fig. 2(b)) the Poynting vector was calculated by integration over the whole space in the far-field. For the calculation of the near-field enhancement spectrum we averaged the electric field closely outside the particle surface and divided by the incident field strength E_0 . The red shift of the dipolar mode in the near-field in comparison to the far-field depends on the damping for large particle sizes where retardation damping is well known.⁵ Plotting the charge distributions at the surface of the NP for excitation with 540 nm and 610 nm light (according to the peak positions in the near-field), one finds that the maxima can be attributed to a vertical mode (dipolar charge distribution in the side view) and an in-plane quadrupolar mode (quadrupolar charge distribution in the bottom view), respectively. The strongly shifting mode from Fig. 2(c) for the smallest NPs in turn can be attributed to an in-plane dipolar mode (dipolar charge distribution in the bottom view) as expected. The spectral positions of the vertical and quadrupolar modes nearly coincide with those of the e-h-pair modes discussed before.

Reference

1. M. A. Lieb and A. J. Meixner, *Opt.Express*, 2001, **8**, 458-474.
2. U. Hohenester and A. Trugler, *Comput. Phys. Commun.*, 2012, **183**, 370-381.
3. <https://refractiveindex.info/> (Accessed 8/2017), following T. A. F. König, P. A. Ledin, J. Kerszulis, M. A. Mahmoud, M. A. El-Sayed, J. R. Reynolds and V. V. Tsukruk, *ACS Nano*, 2014, **8**, 6182-6192.
4. P. B. Johnson and R.-W. Christy, *Phys. Rev. B*, 1972, **6**, 4370.
5. J. Zuloaga and P. Nordlander, *Nano Lett.*, 2011, **11**, 1280-1283.